A new health check of the ozone layer at global and regional scales

Melanie Coldewey-Egbers[1], Diego G. Loyola R.[1], Peter Braesicke[2], Martin Dameris[3], Michel van Roozendael[4], Christophe Lerot[4], and Walter Zimmer[1]

[1]Remote Sensing Technology Institute, German Aerospace Center, Weßling, Germany, [2]Karlsruhe Institute of Technology, Institute for Meteorology and Climate Research, Karlsruhe, Germany, [3]Institute for Physics of the Atmosphere, German Aerospace Center, Weßling, Germany, [4]Belgian Institute for Space Aeronomie BIRA-IASB, Brussels, Belgium

Abstract In this study, we provide a new perspective on the current state of the ozone layer using a comprehensive long-term total ozone data record which has been recently released within the framework of the European Space Agency's Climate Change Initiative. Based on a multivariate regression analysis, we disentangle various aspects of ozone change and variability on global and regional scales, thus enabling the monitoring of the effectiveness of the Montreal Protocol. Given dominant natural variability the expected midlatitude onset of ozone recovery is still not significant and would need additional 5 years of observations to be unequivocally detectable. A regional increase in the tropics is a likely manifestation of a long-term change in El Niño–Southern Oscillation intensity over the last two decades induced by strong El Niño in 1997/1998 and strong La Niña in 2010/2011.

1. Introduction

The stratospheric ozone layer protects organisms and ecosystems on Earth from harmful effects of solar ultraviolet radiation. A strong decline in ozone amounts has been observed, that is, mainly attributable to anthropogenic emissions of ozone-depleting substances (ODSs), e.g., chlorofluorocarbons [*World Meteorological Organization* (*WMO*), 2011]. Since 1987 the Montreal Protocol [*United Nations Environment Programme*, 1986] and its subsequent amendments and adjustments control the production and release of ODSs, thereby starting the process of ozone layer protection. Measurements indicate that stratospheric concentrations of ODSs peaked in the late 1990s and have begun to decrease since the turn of the century [*WMO*, 2011].

Hence, now a key issue is the monitoring of the effectiveness of the Montreal Protocol, i.e., the detection of the expected onset of ozone recovery and its spatial fingerprint. First signs of a turnaround in zonal mean ozone have been reported using satellite as well as ground-based observations [e.g., *Mäder et al.*, 2010; *Salby et al.*, 2011; *Ziemke and Chandra*, 2012; *Kuttippurath et al.*, 2013; *Kyrölä et al.*, 2013; *Chehade et al.*, 2013; *Bourassa et al.*, 2014]. However, statistically significant results are still greatly restricted to very few latitude bands. Large annual and interannual variabilities due to complex feedback mechanisms between chemical and dynamical atmospheric processes hamper the unambiguous detection of ozone recovery. Additionally, the observed increase in the Northern Hemisphere shows also some significant dynamical signature in addition to early signs of recovery [*Dhomse et al.*, 2006; *Wohltmann et al.*, 2007; *Harris et al.*, 2008; *WMO*, 2011].

In order to unravel and quantify the different aspects of ozone variability, high-quality and stable long-term data sets are needed. Within the framework of the European Space Agency's Climate Change Initiative (ESA-CCI) [*Hollmann et al.*, 2013] a coherent and consistent global data record of total ozone has been created. The so-called Global Ozone Monitoring Experiment (GOME)-type total ozone-essential climate variable (GTO-ECV) has been compiled from three European satellite sensors, which provide ozone measurements for the last 18 years. We use this data record to demonstrate its potential to estimate spatially resolved total ozone trends and to analyze decadal ozone variability. We disentangle various aspects of ozone change on global and regional scales using multivariate linear regression. Furthermore, we discuss our ability to detect ozone recovery now and in the near future, which is a central milestone of success for the Montreal Protocol.

Table 1. European Total Ozone Satellite Instrument Characteristics

Parameter	GOME	SCIAMACHY	GOME-2
Data availability	6/1995 to 7/2011[a]	8/2002 to 4/2012	1/2007 to present
Satellite	ESA ERS-2[b]	ESA ENVISAT[c]	EUMETSAT MetOp-A[d]
Spectral coverage	240–790 nm	240–2380 nm	240–790 nm
Spectral resolution	0.2–0.4 nm	0.2–1.5 nm	0.2–0.4 nm
PMD[e] coverage	3 p-PMD	6 p-PMD	15 p-PMD and
	300–800 nm	320–2380 nm	15 s-PMD
			310–790 nm
Viewing geometries	nadir	nadir, limb, occultation	nadir
Ground pixel size	$320 \times 40 \, km^2$	$60 \times 30 \, km^2$	$40 \times 80 \, km^2$
Swath width	960 km	960 km	1920 km
Altitude	785 km	800 km	817 km
Equator crossing	10:30 A.M. LT[f]	10:00 A.M. LT	09:30 A.M. LT
Global coverage	3 days	6 days	almost daily
Reference	*Burrows et al.* [1999]	*Bovensmann et al.* [1999]	*Callies et al.* [2000]

[a]No global coverage since June 2003.
[b]ESA ERS-2: European Space Agency-Second European Remote Sensing Satellite.
[c]ENVISAT: Environmental Satellite.
[d]EUMETSAT MetOp-A: European Organisation for the Exploitation of Meteorological Satellites-Meteorological Operational Satellite-A.
[e]PMD: Polarization Measurement Device detecting polarized light perpendicular (p-) or parallel (s-) to the optical plane.
[f]LT: local time.

2. Data

Three European passive remote sensing instruments GOME (Global Ozone Monitoring Experiment) on board ERS-2 (Second European Remote Sensing Satellite), SCIAMACHY (Scanning imaging absorption spectrometer for atmospheric chartography) on board ENVISAT (Environmental Satellite), and GOME-2 on board MetOp-A (Meteorological Operational Satellite-A) provide global atmospheric composition data for the last 18 years [*Burrows et al.*, 1999; *Bovensmann et al.*, 1999; *Callies et al.*, 2000]. An overview of the most important instrument properties and viewing geometries is given in Table 1. Total ozone is retrieved using (1) the GOME Data Processor (GDP) version 4.X [*Van Roozendael et al.*, 2006; *Lerot et al.*, 2009; *Loyola et al.*, 2011; *Hao et al.*, 2014] and (2) the GOME-type direct fitting version 3 algorithm. The latter is based on the direct fitting of simulated reflectances to the observations in the Huggins band [*Van Roozendael et al.*, 2012; *Lerot et al.*, 2014]. It has been developed within the ESA-CCI, which aims to create long-term and consistent climate data records for a number of essential climate variables (ECVs) including total ozone [*Hollmann et al.*, 2013]. The complete total ozone data records have been reprocessed for the entire time series of all instruments. Intersensor comparisons and ground-based validation indicated that these data records are of superior quality regarding long-term stability and precision [*Lerot et al.*, 2014].

These total ozone data products were the basis for two merged homogeneous data records GTO-ECV GDP and GTO-ECV CCI combining the individual measurements following the approach described in *Loyola et al.* [2009a] and *Loyola and Coldewey-Egbers* [2012]. GOME data are used as a reference standard, and SCIAMACHY and GOME-2 are adjusted using latitudinal and time-dependent correction factors which were determined during instrument overlap periods. These factors account and correct for the generally small remaining intersensor differences [*Lerot et al.*, 2014, Figure 16]. Both data records cover the period from July 1995 to June 2013.

A previous version of GTO-ECV GDP covered the period from July 1995 to December 2009 and was initially used to evaluate atmospheric Chemistry-Climate Model simulations [*Loyola et al.*, 2009a] and for preliminary trend assessment [*Loyola et al.*, 2009b]. Moreover, the data record was used in the last World Meteorological Organization Scientific Assessment of Ozone Depletion [*WMO*, 2011]. An excellent agreement between the GTO-ECV CCI data record and the recently released solar backscatter ultraviolet merged ozone data set version 8.6, based on a comparison of zonal mean total ozone and total ozone anomalies, was found [*Chiou et al.*, 2014]. The mean difference in total ozone is between 0.2% (±0.6%) and 0.8% (±0.7%) depending on the latitude band.

3. Method

The monthly to decadal variability of total ozone is estimated using a multivariate linear regression model that quantifies the relationship between ozone and several explanatory variables describing natural and/or anthropogenic forcings. We adopted the form used in *Vyushin et al.* [2007]:

$$O_3(m) = A + B_0 \cdot m + C \cdot SF(m) + D \cdot QBO30(m)$$
$$+ E \cdot QBO50(m) + F \cdot MEI(m) + X(m). \tag{1}$$

$O_3(m)$ is the monthly mean ozone column, m is the number of months after the initial time (July 1995), and A–F are the model fit coefficients calculated using a standard least squares algorithm. In the case of analyzing the temperature trend (see section 5), $O_3(m)$ is replaced with the monthly mean temperature values $T(m)$.

Seasonal variability is accounted for by expanding the coefficients as, for example,

$$A = A_0 + \sum_{k=1}^{N_A} A_{2k-1} \, \sin(2\pi k \, m/12) + A_{2k} \, \cos(2\pi k \, m/12), \tag{2}$$

with N_A accounting for annual, semiannual, 4 month, and if necessary 3 month variations. We used $N_A = 4$, $N_B = 0$, $N_C = 1$, $N_D = 1$, $N_E = 1$, and $N_F = 0$.

The quasi-biennial oscillation signal is represented by both 30 hPa and 50 hPa equatorial zonally averaged monthly winds (QBO30(m) and QBO50(m)). SF(m) denotes the 10.7 cm radio flux and accounts for the impact of the 11 year solar cycle. MEI(m) is the Multivariate El Niño–Southern Oscillation (ENSO) Index. All covariates have been detrended before the fit in order to ensure that B_0 represents the net trend induced by the covariates and/or unknown processes [*Bodeker et al.*, 1998]. A potential nonnegligible autocovariance of the residuals $X(m)$ is accounted for by applying a Cochrane-Orcutt transformation [*Dhomse et al.*, 2006]. We adopt the common rule that a fit coefficient is statistically significant when its absolute value is greater than 2 times its error (95% confidence interval).

The number of years n^* that is required to detect a trend B_0 with a probability of 90% is calculated following the method described in *Weatherhead et al.* [1998]:

$$n^* = \left[\frac{3.3 \cdot \sigma_X}{|B_0|} \cdot \sqrt{\frac{1+\phi}{1-\phi}} \right]^{\frac{2}{3}}. \tag{3}$$

ϕ is the autocorrelation of the noise term X and σ_X is its variance.

4. Ozone Variability and Trend

The annual mean linear trend coefficients are calculated for both GTO-ECV CCI and GTO-ECV GDP total ozone data records for the period July 1995 to June 2013 from 60°N to 60°S (Figures 1a and 1b). Grey crosses denote regions where the trends are not statistically significant. Estimated trends are positive (yellow and red shading) in major parts of the globe. Small areas indicating nonsignificant negative trends are found in the northern middle latitudes and in the southern Indian Ocean around 30°E–90°E. Statistically significant positive trends around 1% per decade are found in the tropics. Largest positive trends of about 1.5–2% per decade are found in the Northern Hemisphere in the European and North Atlantic region, but they are statistically significant in limited small areas only. In southern middle latitudes significant trends of about 1.5% per decade are found around southern South America, Australia, and New Zealand. Thus, the expected onset of ozone recovery in midlatitudes is still on the edge of detection. However, both GTO-ECV data records show significant positive trends in large parts of the tropics and subtropics, which is discussed in more detail in the subsequent section. The trends in the tropical region differ from those (nonsignificant or just barely positive trends) obtained in other studies [e.g., *Chehade et al.*, 2013], which might be related to the different approaches in selecting the covariates. A sensitivity study yielded that changing the start points of the regression would not have a significant impact on the spatial trend patterns. Concerning the spatial patterns, there is very good agreement between both GTO-ECV versions, indicating that in both cases an accurate ozone retrieval algorithm in combination with an adequate and robust merging approach lead to stable and reliable long-term data records.
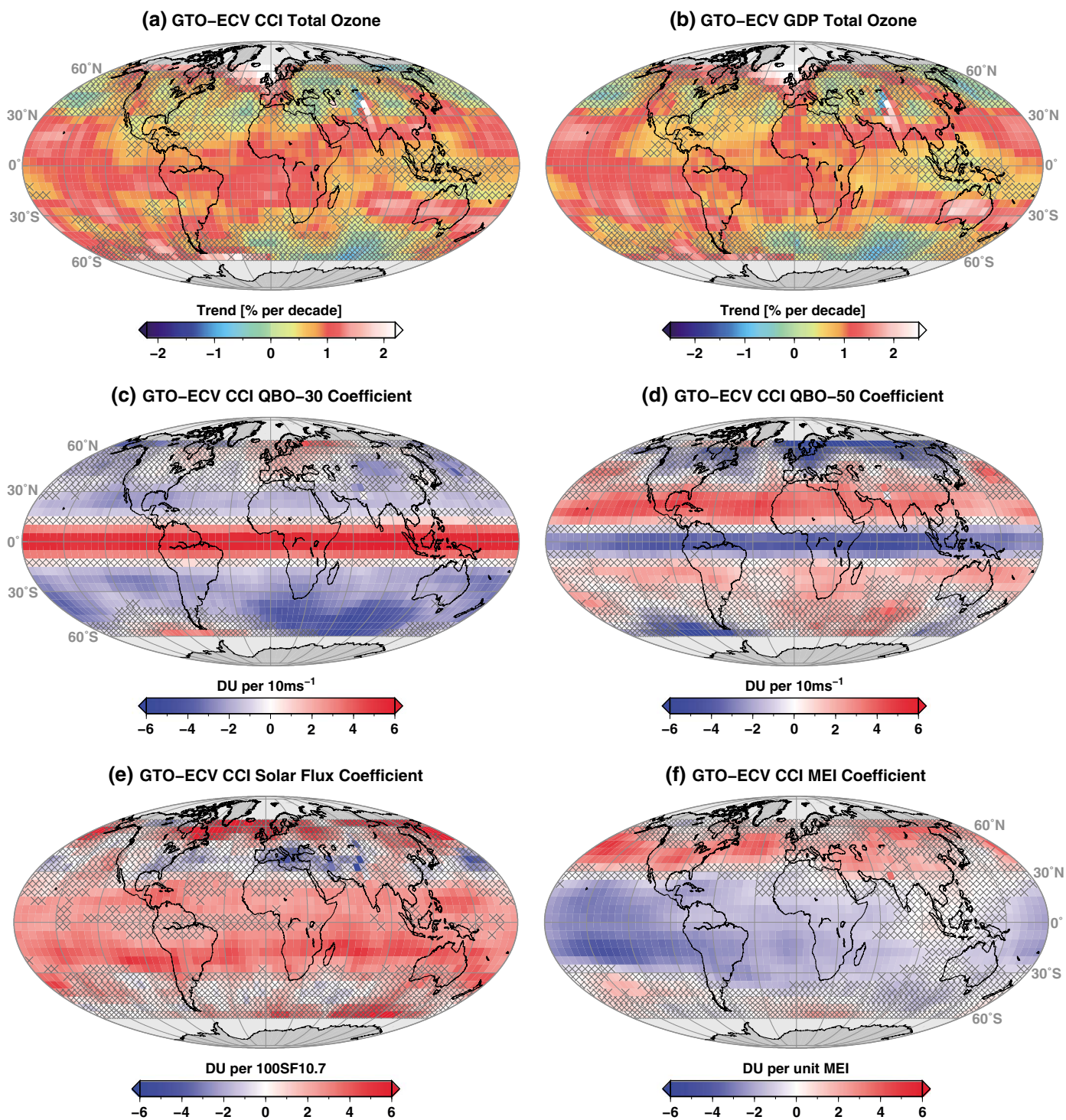
Figure 1. Linear total ozone trend estimates 1995–2013 from satellite data (a) GTO-ECV CCI and (b) GTO-ECV GDP. Note that the scales of the color bars are slightly different. Bottom row: Annual mean regression coefficient estimates per grid point from GTO-ECV CCI data for quasi-biennial oscillation of equatorial zonal winds at (c) 30 hPa and at (d) 50 hPa, (e) the solar cycle, and (f) the Multivariate ENSO Index. Grey crosses denote that the coefficients are not significant at the 95% confidence level.

Figures 1c–1f show the estimated annual mean coefficients as a longitude-latitude map for the GTO-ECV CCI data record for the covariates QBO30, QBO50, the solar flux, and MEI that are main contributors to total ozone variability. QBO30 and QBO50, which are around 90° out of phase, are dominant not only equatorward of 15°N/S but also in the subtropics and midlatitudes. The amplitude is stronger for QBO30 than for QBO50. Positive coefficient estimates (red) indicate an in-phase relation between ozone anomalies and equatorial wind anomalies, i.e., high ozone during westerly winds and low ozone during easterly winds. The increase in ozone in the first case is due to downward transport of ozone-rich air to altitudes where ozone lifetimes are relatively long. Poleward of 20°N/S, the opposite relation is found (blue), i.e., ozone values below the mean during QBO30 westerly phases. These findings are in good agreement with *Baldwin et al.* [2001], *Steinbrecht et al.* [2006] and *Frossard et al.* [2013].

The solar signal coefficients are plotted in Figure 1e. An accurate determination of the solar impact is difficult as the time span of the data record covers only one and a half solar cycles. However, the most important features are visible: (1) a positive correlation between solar activity and ozone in the tropics, i.e., higher ozone levels during solar maxima and vice versa; (2) basically zonally symmetric patterns at low latitudes; and (3) higher amplitudes at northern middle to high latitudes with distinct longitudinal variance due to transport and dynamics [*Steinbrecht et al.*, 2003].

Figure 1f shows the coefficients estimated for the MEI. They are negative and significant for almost the entire tropical zone except the eastern Indian Ocean and Southeast Asia. Maximum values are found in the Pacific. Negative correlations mean that ozone values are higher than the mean during La Niña cold phases and lower during El Niño warm phases, which is in good agreement with earlier studies [*Steinbrecht et al.*, 2006; *Pyle et al.*, 2005; *Oman et al.*, 2013]. Five to 15 Dobson Units of ozone variability can be explained by this phenomenon in those regions. The longitudinal structure in the tropics can be explained with a shift in the convection pattern from east to west during warm El Niño events. Over the eastern Pacific enhanced sea surface temperature (SST) and convection lead to a reduction in tropospheric ozone, whereas toward Indonesia lower SST and reduced convection lead to an increase in tropospheric ozone. Stratospheric columns are more or less zonally invariant [*Ziemke et al.*, 2010]. The area of significance becomes smaller in northern midlatitudes and the correlation reverses, which indicates that during El Niño warm phases meridional circulation is strengthened and transport of ozone-rich air from the tropics to the extratropics is enhanced [*Rieder et al.*, 2013]. Furthermore, enhanced stratosphere-troposphere exchange following El Niño events coincides with an increase in extratropical ozone [*Zeng and Pyle*, 2005]. In southern midlatitudes coefficients are not significant. The zonal distribution of all covariates discussed above is in very good agreement with the results published by *Chehade et al.* [2013].

Next we discuss the measure R^2, which is the ratio of the variance described by the regression to the total variance [*von Storch and Zwiers*, 1999]. If R^2 is close to 1, a large part of the variance can be explained by the regression, whereas R^2 close to zero denote that either random noise is dominating total variance or important explanatory variables are missing in the model. R^2 values for the GTO-ECV CCI global fits are shown in Figure 2a. They indicate that the regression works very well in the tropics, subtropics, and midlatitudes as it explains more than 80% of the variance, which is, however, dominated by the seasonal cycle. Only in southern midlatitudes R^2 values less than 70% occur. Furthermore, a few local minima in R^2, e.g., in the Euro-Atlantic sector and in the northernmost zone of Africa indicate that additional explanatory variables, such as the North Atlantic Oscillation Index or the Antarctic Oscillation Index would have an overall small positive impact on the fidelity of the statistical fit. A sensitivity study yielded a slight increase in R^2 of about 5% in the respective areas when these variables are included.

Figure 2b shows the year in which we can expect to detect a total ozone trend of a given magnitude (see equation (3)). We use the variance and autocorrelation determined from the GTO-ECV CCI measurements, and we use model projections for the first half of this century to obtain a zonal distribution of expected ozone trends, which are smallest in the tropics (~0.5% per decade) and increase toward higher latitudes. Values in middle latitudes of the Southern Hemisphere (1–2% per decade) are expected to be slightly larger than in the Northern Hemisphere (0.7–1.7% per decade).

Figure 2b indicates that detection of changes in the tropics will not be possible before 2030, because the expected trend itself is small and autocorrelation is not negligible. On the other hand, variability is low in this region. Toward higher latitudes the number of years decreases. Early trend detection will be possible from ~2015 onward in some regions in the Southern Hemisphere (20°S poleward), whereas in the Northern
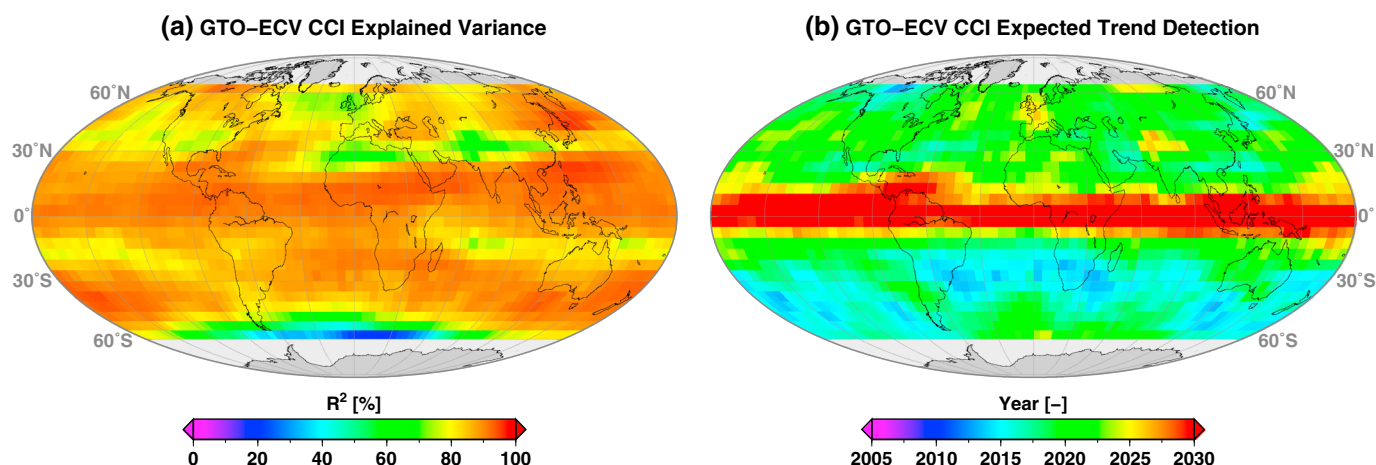
(a) GTO–ECV CCI Explained Variance

(b) GTO–ECV CCI Expected Trend Detection

Figure 2. (a) Explained variance R^2 of regression for GTO-ECV CCI total ozone data record. (b) Estimated year of expected ozone trend detection assuming a zonal mean trend profile estimated from model predictions for the period 1995 through 2050.

Hemisphere stronger interannual and intraannual variabilities lead to longer periods needed to observe a recovery of ozone (trend detection possible from 2020 onward).

As can be readily seen from the results the length of the current GTO-ECV data records covering 18 years is still at the lower end for reliable recovery detection as natural variability still dominates the evolution of total ozone in middle latitudes since the mid-1990s. Therefore, trend estimates presented in Figure 1a are not significant in major parts of the extratropics. Moreover, we have to bear in mind (1) that uncertainty in the regression method influences the determination of the year and (2) that numbers would change if the real trend differs from the predicted one used here. This is the case for the tropics, where the trend of ~1% per decade obtained from the satellite data is larger than the assumed and is thus already statistically significant.

For the polar regions—which cannot be observed throughout the whole year by the satellite measurements—a positive trend of 2% per decade in the Northern Hemisphere and 3% per decade in the Southern Hemisphere is predicted [*WMO*, 2011]. This would imply that trend detection would not be possible before 2020, because variability is also increasing toward the poles.

In the extratropics an anticorrelation between the year of trend detection and the R^2 values (see Figure 2a) is found. In areas where R^2 is lower the number of years increases, as the fit error increases, too.

5. The Role of El Niño–Southern Oscillation

In order to explain the physical mechanisms that control interannual variability and thus small trends in the tropics, we discuss now the link between the ENSO phenomenon and two other important meteorological parameters. Both, lower stratospheric temperature and tropopause pressure, are also known to be correlated with total ozone via chemical and dynamical processes [*Randel and Cobb*, 1994; *Hoinka et al.*, 1996; *Steinbrecht et al.*, 1998, 2003]. Figure 3 (top) illustrates an idealized latitude-pressure cross section of ENSO-related temperature and pressure correlations. It is based on data from the global atmospheric reanalysis project ERA-Interim [*Dee et al.*, 2011] produced and archived by the European Centre for Medium Range Weather Forecasts (ECMWF). Red ellipses indicate warming associated with ENSO warm events; blue areas indicate cooling associated with ENSO warm events. The solid black line indicates a climatological mean lapse-rate tropopause. The dashed arrows indicate the relative change in tropopause pressure (height) for an ENSO warm event. Note that the 100 hPa level (dashed line) intersects the tropopause. The level is below the tropopause in the tropics and above it in the extratropics. The coherent warm anomaly in the subtropics is well captured with a 100 hPa control level (as indicated with dotted lines). Depending on the details only a very small temperature response is seen at the equator, because the transition region from negative to positive temperature anomalies (at 150 hPa) is potentially close. This change in thermal structure relates
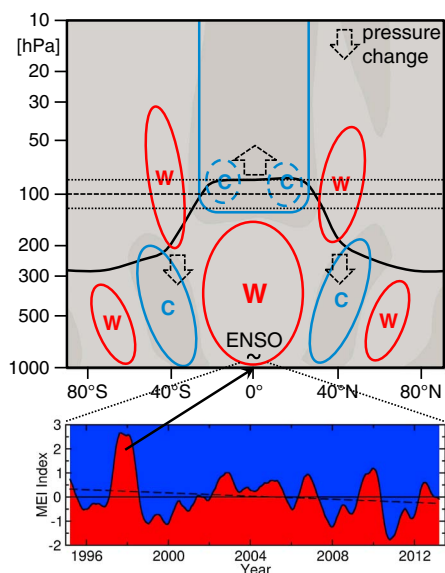
Figure 3. (top) Idealized latitude-pressure cross section of ENSO-related temperature correlations. Red ellipses indicate warming associated with ENSO warm events; blue areas indicate cooling associated with ENSO warm events. The solid black line indicates a climatological mean lapse-rate tropopause. The dashed arrows indicate the relative change in tropopause pressure (height) for an ENSO warm event. (bottom) MEI time series from 1995 to 2013 (black solid line). The dashed line indicates the result from a linear fit through the MEI time series.

well to increased changes in stratosphere-troposphere-exchange during an ENSO warm event [*Zeng and Pyle*, 2005].

As for ozone and in addition to the idealized correlations discussed in the previous paragraph we now determine trends from 1995 to 2013 for the ERA-Interim temperature (at the 100 hPa level) as well as tropopause pressure as a function of latitude and longitude. The altitude of the tropopause can be estimated using the potential temperature (θ) minimum lapse rate. In the tropics the pressure of the $\theta = 395$ K layer can be used as an applicable surrogate for the position of the tropopause.

Temperature trends were obtained in the same way as the ozone trends (see section 3). Annual mean trend estimates are shown in Figure 4a and the corresponding annual mean MEI coefficients in Figure 4b. Temperature trends are positive over the Pacific, southern South America, North Atlantic, and the northern Indian Ocean, the regions where also positive ozone trends are found. The spatial patterns of the annual mean MEI coefficients from the temperature fit and the coefficients obtained from the ozone fit (Figure 1f) are in good agreement. They are negative over the western Pacific. As for ozone, the correlation reverses toward the eastern Pacific and Indonesia, where it is statistically significant. Negative correlation between MEI and temperature means that temperature at 100 hPa is increasing during ENSO cold events (when temperature in the lower tropical troposphere is decreasing), and temperature at 100 hPa is decreasing during ENSO warm events (when temperature in the lower tropical troposphere is increasing). This anticorre-

lation between troposphere and stratosphere is related to enhanced tropical upwelling and a strengthened Brewer-Dobson circulation during El Niño events [*Calvo et al.*, 2010]. Enhanced residual circulation during warm ENSO events is also responsible for positive correlation between temperature and MEI in the middle latitudes [*García-Herrera et al.*, 2006].
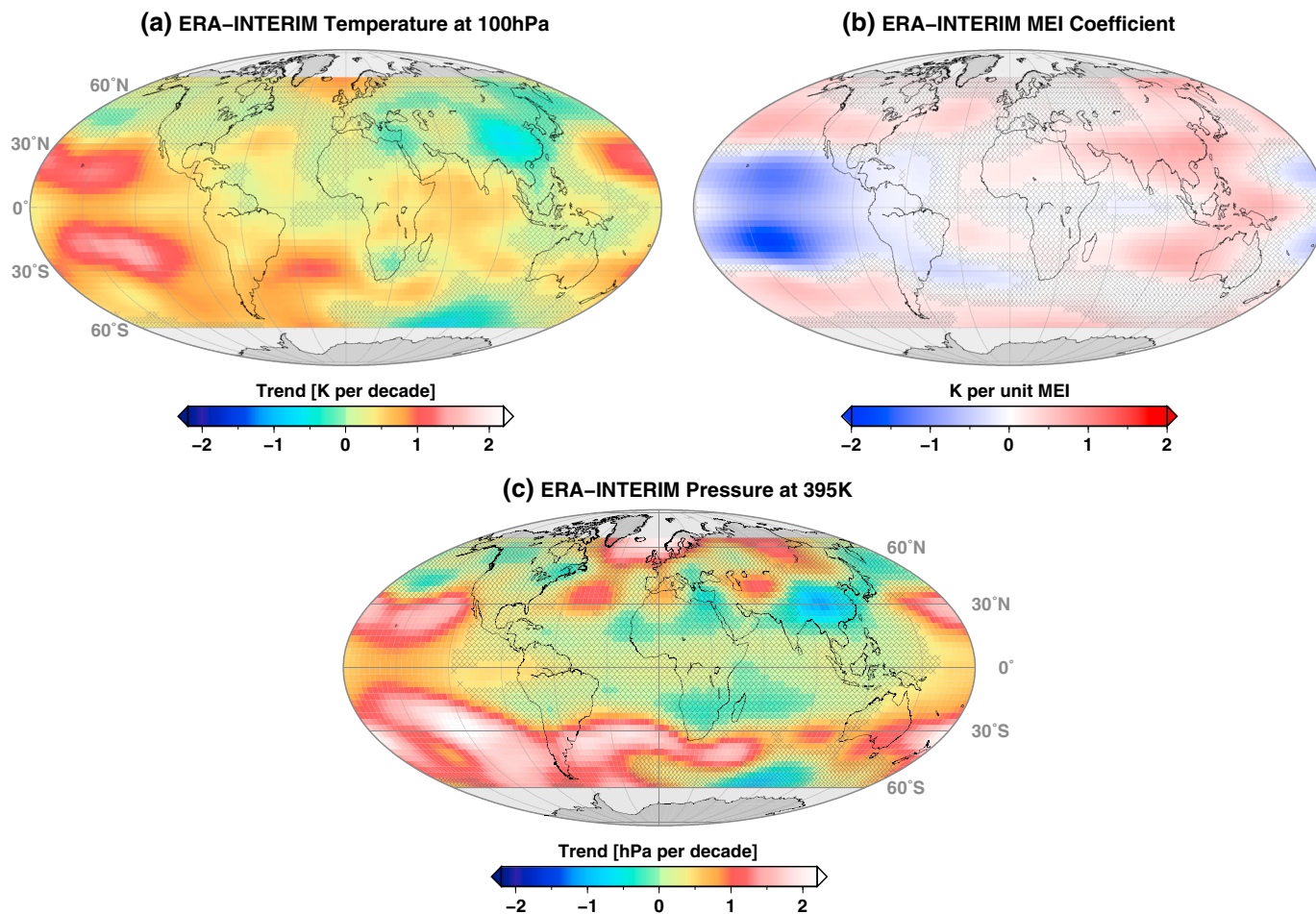
Figure 4c shows the linear trend coefficients for ERA-Interim pressure at 395 K potential temperatures. In contrast to ozone and temperature we used a simple linear fit from 1995 to 2013 for pressure. The latitudinal-longitudinal pattern is similar to the pattern for the temperature trend and shows some agreement with the ozone trend over the Pacific, southern South America, and the North Atlantic region. Positive pressure trends indicate that a descending tropopause is associated with an expanding stratosphere and hence increasing stratospheric ozone levels. In the tropics the changes in pressure are related to ENSO as explained in Figure 3.

With regard to the detected ENSO-related correlations the observed regional trends in the tropics for ozone, temperature, and pressure can now be explained having a look at the MEI time series itself for the period 1995 to 2013 (Figure 3, bottom). We conclude that the strong ENSO warm event 1997/1998 at the beginning of the fit period and the strong ENSO cold event 2010/2011 at the end of the fit period, and hence the apparent negative trend in ENSO toward cold events, induce the derived changes in the atmospheric parameters in this region.

6. Summary and Conclusions

We used the recently released merged GTO-ECV total ozone data record covering the period from June 1995 to June 2013 to calculate spatially resolved total ozone trend and variability patterns. The global long-term data set is based on combined spaceborne observations and enables us to disentangle the various sources

Figure 4. (a) Annual mean temperature trend at 100 hPa obtained from ECMWF ERA-Interim reanalysis data. (b) Corresponding annual mean regression coefficient estimates per grid point for the Multivariate ENSO index. (c) Linear trend coefficient for the pressure level of the 395 K potential temperature. Grey crosses denote that the coefficients are not significant at the 95% confidence level.

of ozone variability and its drivers by multivariate linear regression. The QBO dominates ozone variability in the tropics but has also an impact in the middle latitudes. In addition, the solar cycle and ENSO contribute to decadal and interannual changes.

The linear trends in total ozone during this period are positive in major parts of the globe, but statistical uncertainty is large, in particular in the middle latitudes. Largest positive trends of about 1.5–2.0% per decade are found in the European and North Atlantic region. We conclude that given dominant natural variability over last two decades the expected midlatitude ODSs related onset of ozone recovery would need at least additional 5 years of observations to be unequivocally detectable. Longer periods are required in high latitudes, where approximately 10–20 additional years are needed to draw authoritative conclusions.

In the tropics expected ozone changes are smaller than in other regions, as the evolution of tropical ozone depends on the balance between predicted upper stratospheric increases and lower stratospheric decreases [*WMO*, 2011]. In this area we identify regional trend patterns for ozone (~1% per decade) and temperature, which are mainly attributable to a long-term change in El Niño–Southern Oscillation intensity and which are linked to a changing position of the tropopause.

Our results clearly indicate a need for continuous monitoring of ozone and an extension of the current data records using future missions in order to (1) detect the expected success of the Montreal Protocol and (2) achieve a better understanding of the interaction and feedback mechanisms between ozone and climate change.

References

Baldwin, M. P., et al. (2001), The quasi-biennial oscillation, *Rev. Geophys.*, *39*, 179–229.

Bodeker, G. E., I. S. Boyd, and W. A. Matthews (1998), Trends and variability in vertical ozone and temperature profiles measured by ozonesondes at Lauder, New Zealand: 1986–1996, *J. Geophys. Res.*, *103*(D22), 28,661–28,681, doi:10.1029/98JD02581.

Bourassa, A. E., D. A. Degenstein, J. M. Zawodny, E. Kyrölä, C. A. McLinden, C. E. Sioris, and C. Z. Roth (2014), Trends in stratospheric ozone derived from merged SAGE II and Odin-OSIRIS satellite observations, *Atmos. Chem. Phys. Discuss.*, *14*, 7113–7140, doi:10.5194/acpd-14-7113-2014.

Bovensmann, H., J. P. Burrows, M. Buchwitz, J. Frerick, S. Noel, V. V. Rozanov, K. V. Chance, and A. P. H. Goede (1999), SCIAMACHY: Mission objectives and measurement modes, *J. Atmos. Sci.*, *56*(2), 127–150.

Burrows, J. P., et al. (1999), The Global Ozone Monitoring Experiment (GOME): Mission concept and first scientific results, *J. Atmos. Sci.*, *56*(2), 151–175.

Callies, J., E. Corpaccioli, M. Eisinger, A. Hahne, and A. Lefebvre (2000), GOME-2—Metop's second generation sensor for operational ozone monitoring, *ESA Bull.*, *102*, 28–36.

Calvo, N., R. R. Garcia, W. J. Randel, and D. R. Marsh (2010), Dynamical mechanism for the increase in tropical upwelling in the lowermost tropical stratosphere during warm ENSO events, *J. Atmos. Sci.*, *67*, 2331–2340, doi:10.1175/2010JAS3433.1.

Chehade, W., J. P. Burrows, and M. Weber (2013), Total ozone trends and variability during 1979–2012 from merged datasets of various satellites, *Atmos. Chem. Phys. Discuss.*, *13*(11), 30,407–30,452, doi:10.5194/acpd-13-30407-2013.

Chiou, E. W., P. K. Bhartia, R. D. McPeters, D. G. Loyola, M. Coldewey-Egbers, V. E. Fioletov, M. van Roozendael, C. Lerot, R. Spurr, and S. M. Frith (2014), Comparison of profile total ozone from SBUV(v8.6) with GOME-type and ground-based total ozone for 16-yr period (1996 to 2011), *Atmos. Meas. Tech.*, *7*, 1681–1692, doi:10.5194/amt-7-1681-2014.

Dee, D. P., et al. (2011), The ERA-Interim reanalysis: Configuration and performance of the data assimilation system, *Q. J. R. Meteorol. Soc.*, *137*(656), 553–597, doi:10.1002/qj.828.

Dhomse, S., M. Weber, I. Wohlmann, M. Rex, and J. P. Burrows (2006), On the possible causes of recent increases in northern hemispheric total ozone from a statistical analysis of satellite data from 1979 to 2003, *Atmos. Chem. Phys.*, *6*, 1165–1180.

Frossard, L., H. E. Rieder, M. Ribatet, J. Staehelin, J. A. Maeder, S. Di Rocco, A. C. Davison, and T. Peter (2013), On the relationship between total ozone and atmospheric dynamics and chemistry at mid-latitudes—Part 1: Statistical models and spatial fingerprints of atmospheric dynamics and chemistry, *Atmos. Chem. Phys.*, *13*(1), 147–164, doi:10.5194/acp-13-147-2013.

García-Herrera, R., N. Calvo, R. R. Garcia, and M. A. Giorgetta (2006), Propagation of ENSO temperature signals into the middle atmosphere: A comparison of two general circulation models and ERA-40 reanalysis data, *J. Geophys. Res.*, *111*, D06101, doi:10.1029/2005JD006061.

Hao, N., M. E. Koukouli, A. Inness, P. Valks, D. G. Loyola, W. Zimmer, D. S. Balis, I. Zyrichidou, M. Van Roozendael, C. Lerot, and R. J. D. Spurr (2014), GOME-2 total ozone columns from MetOp-A/MetOp-B and assimilation in the MACC system, *Atmos. Meas. Tech. Discuss.*, *7*, 2259–2299, doi:10.5194/amtd-7-2259-2014.

Harris, N. R. P., et al. (2008), Ozone trends at northern mid- and high latitudes—A European perspective, *Ann. Geophys.*, *26*, 1207–1220.

Hoinka, K. P., H. Claude, and U. Köhler (1996), On the correlation between tropopause pressure and ozone above central Europe, *Geophys. Res. Lett.*, *23*(14), 1753–1756, doi:10.1029/96GL01722.

Hollmann, R., et al. (2013), The ESA climate change initiative: Satellite data records for essential climate variables, *Bull. Am. Meteorol. Soc.*, *94*, 1541–1552, doi:10.1175/BAMS-D-11-00254.1.

Kuttippurath, J., F. Lefèvre, J.-P. Pommereau, H. K. Roscoe, F. Goutail, A. Pazmiño, and J. D. Shanklin (2013), Antarctic ozone loss in 1979–2010: First sign of ozone recovery?, *Atmos. Chem. Phys.*, *13*, 1625–1635, doi:10.5194/acp-13-1625-2013.

Kyrölä, E., M. Laine, V. Sofieva, J. Tamminen, S.-M. Päivärinta, S. Tukiainen, J. Zawodny, and L. Thomason (2013), Combined SAGE II-GOMOS ozone profile data set 1984–2011 and trend analysis of the vertical distribution of ozone, *Atmos. Chem. Phys.*, *13*(21), 10,645–10,658, doi:10.5194/acp-13-10645-2013.

Lerot, C., M. van Roozendael, J. van Geffen, J. van Gent, C. Fayt, R. Spurr, G. Lichtenberg, and A. von Bargen (2009), Six years of total ozone column measurements from SCIAMACHY nadir observations, *Atmos. Meas. Tech.*, *2*, 87–98.

Lerot, C., et al. (2014), Homogenized total ozone data records from the European sensors GOME/ERS-2, SCIAMACHY/Envisat and GOME-2/MetOp-A, *J. Geophys. Res. Atmos.*, *119*(3), 1639–1662, doi:10.1002/2013JD020831.

Loyola, D., and M. Coldewey-Egbers (2012), Multi-sensor data merging with stacked neural networks for the creation of satellite long-term climate data records, *EURASIP J. Adv. Signal Process.*, *2012*(1), 1–10, doi:10.1186/1687-6180-2012-91.

Loyola, D. G., M. Coldewey-Egbers, M. Dameris, H. Garny, A. Stenke, M. van Roozendael, C. Lerot, D. Balis, and M. Koukouli (2009a), Global long-term monitoring of the ozone layer—A prerequisite for predictions, *Int. J. Remote Sens.*, *30*(15–16), 4295–4318, doi:10.1080/01431160902825016.

Loyola, D. G., M. Coldewey-Egbers, W. Zimmer, M. Koukouli, D. Balis, C. Lerot, M. van Roozendael, and M. Dameris (2009b), Total ozone trends derived from the 14-years merged GOME/SCIAMACHY/GOME-2 data record, in *Proc. 'Atmospheric Science Conference', Barcelona, Spain, 7–11 September 2009 (ESA SP-676, November 2009)*, European Space Agency, Paris, France.

Loyola, D. G., M. E. Koukouli, P. Valks, D. S. Balis, N. Hao, M. van Roozendael, R. J. D. Spurr, W. Zimmer, S. Kiemle, C. Lerot, and J.-C. Lambert (2011), The GOME-2 total column ozone product: Retrieval algorithm and ground-based validation, *J. Geophys. Res.*, *116*, D07302, doi:10.1029/2010JD014675.

Mäder, J. A., J. Staehelin, T. Peter, D. Brunner, H. E. Rieder, and W. A. Stahel (2010), Evidence for the effectiveness of the Montreal Protocol to protect the ozone layer, *Atmos. Chem. Phys.*, *10*(24), 12,161–12,171, doi:10.5194/acp-10-12161-2010.

Oman, L. D., A. R. Douglass, J. R. Ziemke, J. Rodriguez, D. W. Waugh, and J. E. E. Nielsen (2013), The ozone response to ENSO in Aura satellite measurements and a chemistry-climate simulation, *J. Geophys. Res. Atmos.*, *118*, 965–976, doi:10.1029/2012JD018546.

Pyle, J. A., P. Braesicke, and G. Zeng (2005), Dynamical variability in the modelling of chemistry-climate interactions, *Faraday Discuss.*, *130*, 27–39, doi:10.1039/B417947C.

Randel, W. J., and J. B. Cobb (1994), Coherent variations of monthly mean total ozone and lower stratospheric temperature, *J. Geophys. Res.*, *99*(D3), 5433–5447, doi:10.1029/93JD03454.

Rieder, H. E., L. Frossard, M. Ribatet, J. Staehelin, J. A. Maeder, S. Di Rocco, A. C. Davison, T. Peter, P. Weihs, and F. Holawe (2013), On the relationship between total ozone and atmospheric dynamics and chemistry at mid-latitudes—Part 2: The effects of the El Niño/Southern Oscillation, volcanic eruptions and contributions of atmospheric dynamics and chemistry to long-term total ozone changes, *Atmos. Chem. Phys.*, *13*(1), 165–179, doi:10.5194/acp-13-165-2013.

Salby, M., E. Titova, and L. Deschamps (2011), Rebound of Antarctic ozone, *Geophys. Res. Lett.*, *38*, L09702, doi:10.1029/2011GL047266.

Steinbrecht, W., H. Claude, U. Köhler, and K. P. Hoinka (1998), Correlations between tropopause height and total ozone: Implications for long-term changes, *J. Geophys. Res.*, *103*, 19,183–19,192, doi:10.1029/98JD01929.

Steinbrecht, W., B. Hassler, H. Claude, P. Winkler, and R. S. Stolarski (2003), Global distribution of total ozone and lower stratospheric temperature variations, *Atmos. Chem. Phys.*, *3*, 1421–1438.

Steinbrecht, W., et al. (2006), Interannual variation patterns of total ozone and lower stratospheric temperature in observations and model simulations, *Atmos. Chem. Phys.*, *6*, 349–374, doi:10.5194/acp-6-349-2006.

United Nations Environment Programme (1986), Handbook for the Montreal Protocol on substances that deplete the ozone layer, ozone secretariat—United Nations Environment Programme. [Available at http://ozone.unep.org/Publications/MP_Handbook/index.shtml.]

Van Roozendael, M., et al. (2006), Ten years of GOME/ERS-2 total ozone data. The new GOME data processor (GDP) version 4: 1. Algorithm description, *J. Geophys. Res.*, *111*, D14311, doi:10.1029/2005JD006375.

Van Roozendael, M., et al. (2012), Sixteen years of GOME/ERS-2 total ozone data: The new direct-fitting GOME Data Processor (GDP) version 5—Algorithm description, *J. Geophys. Res.*, *117*, D03305, doi:10.1029/2011JD016471.

von Storch, H., and F. W. Zwiers (1999), *Statistical Analysis in Climate Research*, Cambridge Univ. Press, New York.

Vyushin, D. I., V. E. Fioletov, and T. G. Shepherd (2007), Impact of long-range correlations on trend detection in total ozone, *J. Geophys. Res.*, *112*, D14307, doi:10.1029/2006JD008168.

Weatherhead, E. C., et al. (1998), Factors affecting the detection of trends: Statistical considerations and applications to environmental data, *J. Geophys. Res.*, *103*(D14), 17,149–17,161.

Wohltmann, I., R. Lehmann, M. Rex, D. Brunner, and J. A. Maeder (2007), A process-oriented regression model for column ozone, *J. Geophys. Res.*, *112*, D12304, doi:10.1029/2006JD007573.

World Meteorological Organization (WMO) (2011), Scientific assessment of ozone depletion: 2010, *Report No. 52*, WMO Global Ozone Research and Monitoring Project, Geneva, Switzerland.

Zeng, G., and J. A. Pyle (2005), Influence of El Niño Southern Oscillation on stratosphere/troposphere exchange and the global tropospheric ozone budget, *Geophys. Res. Lett.*, *32*, L01814, doi:10.1029/2004GL021353.

Ziemke, J. R., and S. Chandra (2012), Development of a climate record of tropospheric and stratospheric column ozone from satellite remote sensing: Evidence of an early recovery of global stratospheric ozone, *Atmos. Chem. Phys.*, *12*, 5737–5753, doi:10.5194/acp-12-5737-2012.

Ziemke, J. R., S. Chandra, L. D. Oman, and P. K. Bhartia (2010), A new ENSO index derived from satellite measurements of column ozone, *Atmos. Chem. Phys.*, *10*(8), 3711–3721, doi:10.5194/acp-10-3711-2010.